Scanning Near-Field Optical Microscope for the Characterization of Optical Integrated Waveguides

X. Borrisé, D. Jiménez, N. Barniol, F. Pérez-Murano, and X. Aymerich

***Abstract*—A scanning near-field optical microscope for the characterization of optical integrated devices has been developed. Compatible with a normal optical characterization setup the experimental setup allows a tapered uncoated optical fiber to scan the optical device with constant height by means of a shear force control using a tuning fork, and to obtain the evanescent field emerging from it. In this way, images showing simultaneously the topography with lateral resolution better than 10 nm and vertical resolution of 1 nm, and the optical field distribution have been obtained. Images obtained over rib waveguides show the guided mode intensity distribution, allowing characterization of the propagation of the light in the device for up to 1 mm. Identification of the guided mode propagation has been achieved by comparing the images with computer simulations. Measurement of the experimental decay lengths of the evanescent field obtained by the microscope allows a determination of the effective refractive index of the structure to be made.**

***Index Terms*—Integrated optics, optical measurements, optical waveguides, refractive index, scanning near-field optical microscopy (SNOM).**

I. Introduction

OPTICAL devices based on integrated waveguides are crucial for the future development of optical communication systems. Further technological developments for the fabrication of these devices require increased information coming from optical characterization. Standard optical characterization techniques are based on analyzing the light at the output of the waveguide and information about propagation inside the waveguide is partially lost. On the other hand, scanning near field optical microscopy, SNOM [1], allows one to analyze the light propagation along the waveguide with nanometer resolution, by collecting the evanescent field at the surface of the waveguide [2]. This method is nondestructive, no special preparation of the sample is required, and is compatible with standard optical measurements.

Images of the evanescent field at the surface of the waveguide are created by scanning a sharp optical fiber tip kept at few nanometers over the surface. With this method, a high resolution topographic image of the waveguide is simultaneously obtained. This allows one to relate light propagation to topographic features of the sample. Moreover, by measuring the decay length of the evanescent field, information on the effective refractive index of the waveguide at any point of the structure can also be obtained.

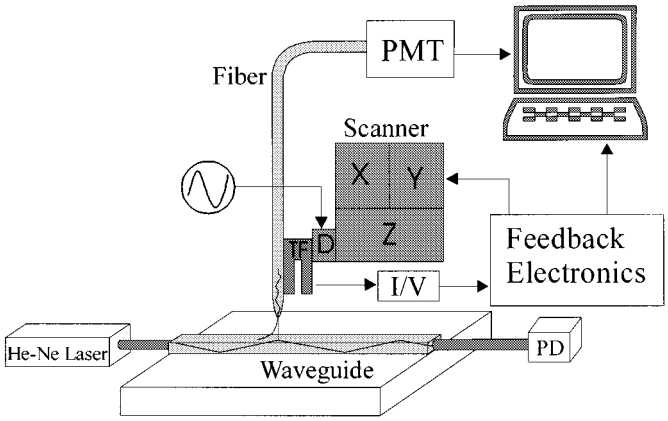

Fig. 1. Experimental setup: PD—photodiode to characterize the light coming out from the waveguide, TF—tuning fork, D—piezoelectric dither, and I/V—current voltage converter to detect the change in amplitude of the tuning fork, PMT—photomultiplier to amplify the evanescent field signal for the optical image.

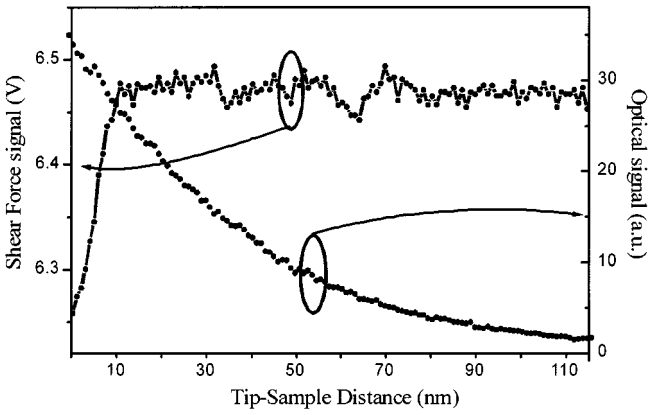

Fig. 2. Shear force signal and optical signal versus tip sample distance. A decreasing of the tuning fork signal is detected, as well as the increasing of the optical signal due to the presence of the evanescent field.

We have developed an instrument that presents important advantages over previously reported works with the same aim of characterizing optical properties of waveguide-based devices [3]–[9]. First, the use of an external shear force based feedback control instead of the optical signal coming from the tip allows complete separation topography from the optical properties, unlike the traditional PSTM systems used by Tsai *et al.* [3], Otshu *et al.* [4], and Hosain *et al.* [5]. Second, the shear force detection method is nonoptical, contrary to the reported by Bourzeix *et al.* [6], Naghski *et al.* [7], Mannoni *et al.* [8], and van Hulst *et al.* [9]. In this way, we avoid the stray light coming from the laser

Manuscript received April 12, 1999; revised October 1, 1999. This work was supported by the CICYT Project TIC98-0499 of the Spanish Government.

The authors are with the Departament d'Enginyeria Electrònica, Edifici Cn, Universitat Autònoma de Barcelona, Bellaterra E-08193, Spain (e-mail: xevi@cc.uab.es).

Publisher Item Identifier S 0733-8724(00)02190-3.

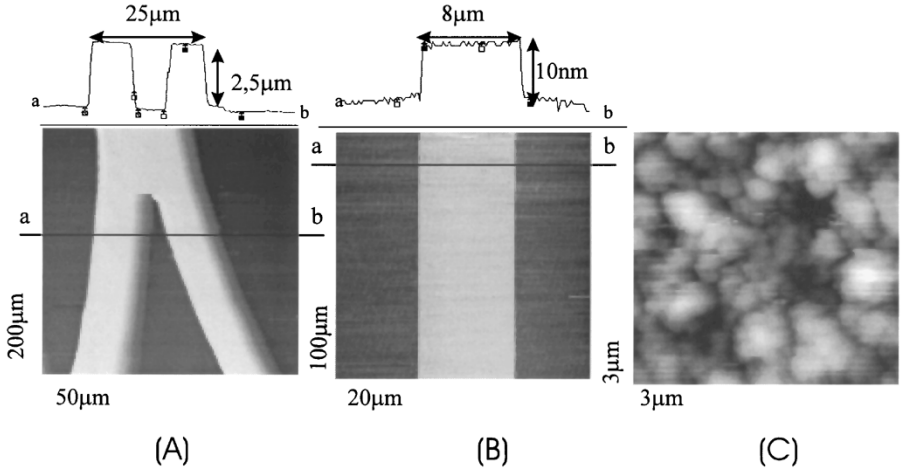

Fig. 3. Topographic images of integrated optical structures. (A) 50 μm × 200 μm image of the splitting point of an ARROW waveguide interferometer. A profile extracted from the image is shown on top. (B) 20 μm × 100 μm image of a Si_3N_4 rib waveguide, a profile extracted from the image is shown on top. (C) 3 μm × 3 μm image of the surface of an ARROW waveguide; the rms roughness of the surface is 10 nm.

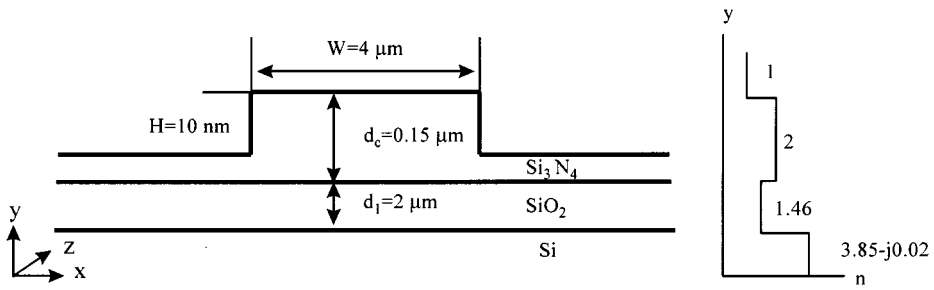

Fig. 4. Structure and index profile of the Si_3N_4 waveguide studied. A 150-nm Si_3N_4 core is between the air and a 2-μm SiO_2 layer. The light confinement in the lateral direction is achieved by a 10-nm RIE in the Si_3N_4 layer.

diode used for the optical detection of the tip oscillation and also provides an instrument capable of performing large scan ranges without any misalignments due to scanning with the tip instead of with the sample. Third, because the sample is fixed, the images obtained reflect the true propagation field along the waveguide and not just a mapping of the effective refractive index of the waveguide as the works of Mannoni *et al.* [8] and Hosain *et al.* [5]. In their instruments the scanning is performed by the sample, so the coupled light is not stationary.

II. Experimental Setup

The developed SNOM follows a stand alone design; the scanner and the tip are mounted in a screw driven tripod for the coarse approach of the tip over the sample. The whole scanner is placed in the optical setup where the light coming from a 633-nm laser is coupled into the waveguide by means of either an optical fiber or by a microscope objective (Fig. 1). A photodiode detects the light coming out from the waveguide in order to assure a good light coupling. The whole scanner is 12 cm long × 5 cm high and 8 cm wide. It can be easily manipulated over a 10 mm square range with additional micrometric screws. The sample holder is also mounted on a micrometer screw, allowing the study of 3 cm long × 2 cm wide samples. The optical fiber tip is positioned over this wide scan region with the aid of an optical microscope and a CCD camera, making it possible to find the structures to be characterized easily. Images up to 300 μm × 150 μm range in the plane of the sample and 4 μm in the vertical direction are obtained by using piezoelectric bimorph plates for the tip scanning. The use of a piezoelectric bimorph plate configuration, instead of the normal piezoelectric tube scanner, provides a much higher scan range with a more compact design and consequently more robust performance against mechanical vibrations, thermal drift, and nonlinearities of the piezoceramics. (A piezoelectric with tube configuration should be 15 cm long.) To compensate the nonidealities of the piezoelectric ceramics (nonlinearity, creep, and histeresy) a closed loop feedback system is implemented in our setup through an additional optical detection of the piezo movement.

The tip sample distance control is based on shear force detection with a tuning fork [10]. This shear force detection system allows one to follow the topography with an accuracy better than 1 nm in height and 10 nm in the lateral direction. Shear force versus tip sample distance curve is presented in Fig. 2 showing both the oscillation amplitude of the tuning fork and the optical signal collected by the tapered fiber tip. From this curve, the exponential decay of the evanescent field is clearly seen.

The signal collected with the tapered optical fiber tip is acquired by a photomultiplier (PMT) and monitored with the computer, obtaining the optical image of the sample. Simultane-

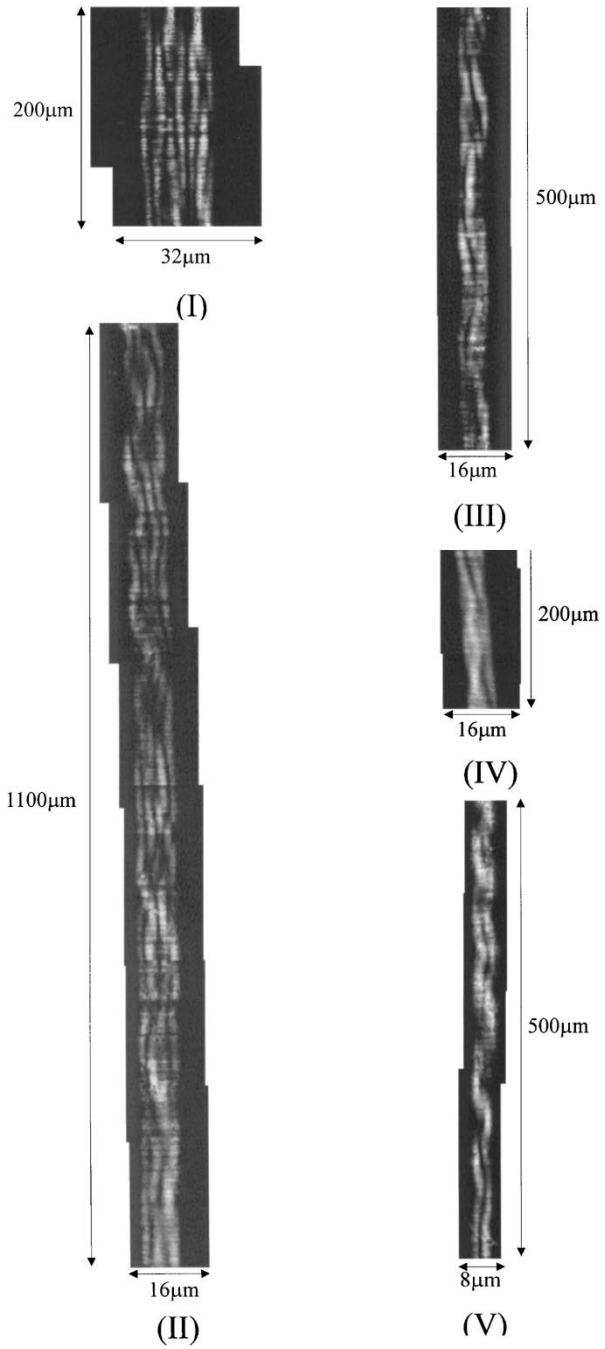

Fig. 5. SNOM images of the evanescent field showing the modal propagation along the waveguide, for different waveguide widths, W: (I) $W = 15\ \mu$m, image dimensions: 32 μm × 200 μm. (II) $W = 8\ \mu$m, image dimensions: 16 μm × 1100 μm. (III) $W = 6\ \mu$m, image dimensions: 16 μm × 500 μm; (IV) $W = 4\ \mu$m, image dimensions: 16 μm × 200 μm. (V) $W = 3\ \mu$m, image dimensions: 8 μm × 500 μm.

ously, by monitoring the Z voltage applied to the piezo, the topographical image is recorded.

The optical fiber used for imaging is a silica single mode fiber at 630 nm (3M FS-SN-3224). Two procedures were used for sharpening the fiber: a chemical etching in a HF (48%) solution and a pulling and heating mechanism [11]. In the chemical etching, after removing 5 mm of the protecting cover, the fiber was immersed in the HF solution for 40 min. Because of the different etch ratings of the core and the cladding of the fiber, a sharp tip is obtained. In the pulling and heating mechanism, a commercial micropipette puller adapted for tapering fibers was used (Sutter Instruments P2000). No coating was applied to the fibers after sharpening. Both types of fabricated fibers lead to similar results.

III. Results and Discussion

The following information on the optical waveguides devices is obtained with the present setup: 1) topography and structure of the device with high spatial resolution (10 nm laterally and 1 nm in height), 2) modal field shape of the propagation of the light in the waveguide simultaneously with the topographic

image, and 3) a mapping of the effective refraction index of the optical waveguide.

A. Topographic Characterization

A precise characterization of the topographic features of the waveguide is relevant in order to understand deviations of the propagation of the light from an ideal waveguide structure. Height, width, side wall angles and the surface roughness of rib waveguides have been obtained, as well as the presence of defects, dust, or anomalous features that can affect light propagation. Fig. 3 shows three topographic images of different structures. In Fig. 3(a), an image of the splitting point of an antiresonant reflection optical waveguide (ARROW) interferometer [12]. From the extracted profile, vertical and lateral dimensions of the structure are determined with precision.

When the rib of the waveguide is of the order of nanometers, a high resolution topographic characterization is needed. In Fig. 3(b), we show a rib waveguide made of Si_3N_4 with a 10-nm step (see profile above the image) and 4-μm width. The specifications of the technological process predicts a value of 4 nm. This difference implies important changes on the light propagation characteristics, modifying the designed monomode behavior of the waveguide to a multimode one.

In Fig. 3(c) a high resolution topographic image of the surface (3 μm $\times$ 3 μm) of an ARROW waveguide is shown, allowing an evaluation of the roughness of the surface. (The root-mean-square (rms) value is 10 nm.) This topographical information can be used for studying the effect of surface roughness on light transmission and its influence on waveguide losses.

B. Modal Propagation

Fig. 4 shows the structure and refractive index profile of a Si_3N_4 waveguide used to study the modal light propagation. On a 2-μm SiO_2 layer, a Si_3N_4 layer of 150 nm thick has been grown. A reactive ion etching of the Si_3N_4 layer provides a 10-nm–height rib, used to confine the light in the lateral direction. The upper cladding is the air, where the evanescent field is directly collected by the fiber tip. Waveguides have been fabricated with widths varying from 3 to 15 μm. From theoretical calculations a multimodal behavior for all the waveguides is expected.

In Fig. 5 the evanescent field optical images of these waveguides are presented. Images show the increase of the number of lateral modes with increasing the width of the waveguide. Notice that the distance in the direction of light propagation is very large. This is achieved by changing the position of the whole scanner in order to obtain connected images that reveal the modal propagation along more than 1 mm of the structure. In order to have a complete view of the total scanned area, the images have been compressed in the direction of propagation. The same procedure can be applied to more complex structures, in order to get valuable information at special points of the structure such as splitting points and sensor or coupling regions.

Comparison with simulations has been performed in order to determine the modal distribution along the waveguide. In Fig. 6(a), the experimental image of the evanescent field of a 4-μm-wide Si_3N_4 waveguide is compared with a finite difference beam propagation method (BPM-simulation) of the same structure [Fig. 6(b)]. From simulations we deduce that this structure supports four lateral modes, and that the beating period of 63.4 μm corresponds to the propagation of the lateral TE_0 and TE_2 excited modes. From similar simulations, the number of modes as a function of waveguide width are presented in Table I.

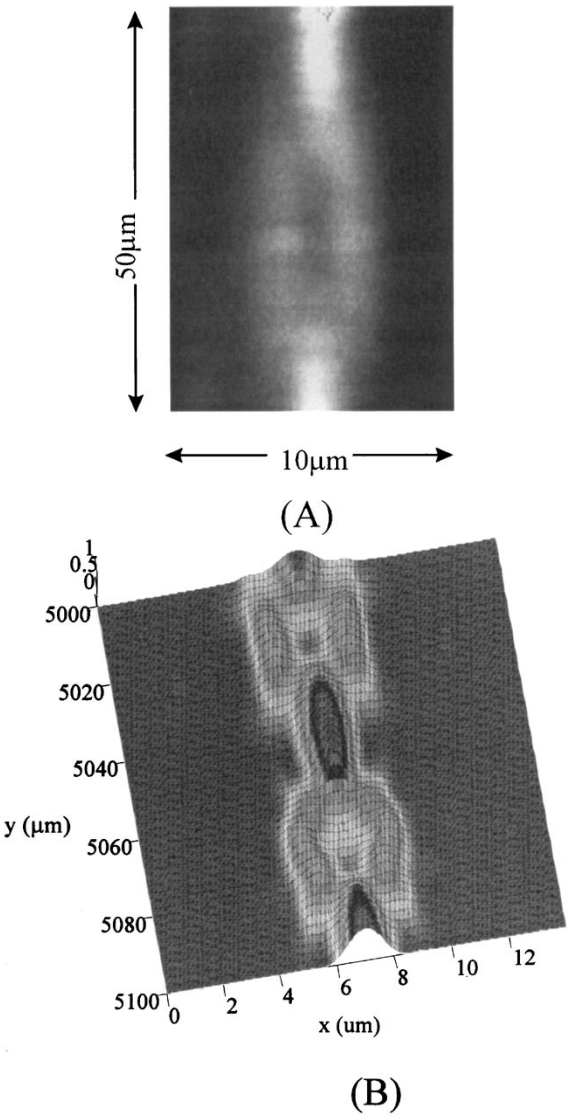

Fig. 6. Optical distribution of a 4 μm wide Si_3N_4 rib waveguide: (a) experimental SNOM image of 10 μm $\times$ 50 μm and (b) intensity of the optical field at the surface of the waveguide obtained from BPM simulation. Dimensions: 14 μm $\times$ 100 μm.

TABLE I
NUMBER OF MODES DEPENDING ON THE WAVEGUIDE WIDTH FOR 10-nm HIGH RIB Si_3N_4 WAVEGUIDES

Waveguide width	3 μm	4 μm	6 μm	8 μm	15 μm
No. of lateral modes	3	4	5	7	13
No. of image in Fig. 6	V	IV	III	II	I

C. Evanescent Field Determination

It is also possible to perform a mapping of the effective refractive index of the optical waveguide, n_e. When the distance

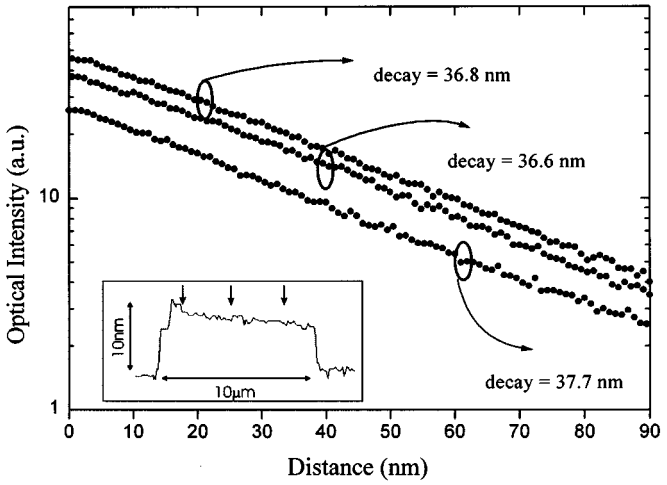

Fig. 7. Optical signal versus tip to sample distance over three different places along the waveguide showing an exponential behavior due to the evanescent field. Inset: topographic profile of the waveguide showing the positions used to perform the approach curves.

TABLE II
DECAY LENGTH AND CALCULATED EFFECTIVE REFRACTIVE INDEX OBTAINED FROM THE APPROACH CURVES OF FIG. 7

	Theoretical	SNOM Data			
		Curve 1	Curve 2	Curve 3	Mean Value
Decay Length	36.9nm	36.8 nm	36.6 nm	37.7 nm	37.0 nm
Eff. Refr. Index	1.693	1.695	1.701	1.669	1.698

between the tip and the sample, z, is changed (applying a voltage to the Z piezo) the optical signal changes accordingly to

$$I(z) = I_0 \exp\left(\frac{-z}{d}\right) \tag{1}$$

where d is the evanescent field decay length. This decay length is related with the effective refractive index by the following expression:

$$d = \frac{\lambda}{4\pi\sqrt{n_e^2 - 1}} \tag{2}$$

where λ is the light wavelength.

Fig. 7 presents optical versus distances curves at three different positions of a waveguide (see inset in Fig. 7). The curves show the exponential behavior expected from an evanescent field (1). From these curves, we obtain a decay length of 37.0 nm (average value from Table II), which is in perfect agreement with the theoretical decay length for transverse electrical mode TE_0, 36.9 nm. The effective refractive index deduced from this decay length is 1.689.

IV. CONCLUSION

A SNOM microscope specifically designed for the characterization of optical waveguides has been developed. The optical field distribution of the light in the waveguide is obtained from the acquisition of the evanescent field. In addition, simultaneously to the optical images the SNOM provides a high resolution characterization of the topographic features of the waveguide. Measurements of surface roughness, rib height, modal propagation, and decay length have been performed and compared with theoretical values, indicating that the SNOM is a very useful and suitable technique for the characterization of optical integrated waveguides.

ACKNOWLEDGMENT

The authors wish to thank Prof. N. van Hulst from the University of Twente, The Netherlands, for the technical support in developing the SNOM and for the provided pulled tips and C. Domínguez from the IMB-CNM for providing the samples.

REFERENCES

[1] E. Betzig, J. K. Trautman, T. D. Harris, J. S. Weiner, and R. L. Kostelak, "Breaking the diffraction barrier: Optical microscopy on a nanometric scale," *Science*, vol. 251, pp. 1468–1470, Mar. 1991.
[2] M. L. M. Balistreri, X. Borrisé, J. P. Korterik, and N. F. van Hulst, "Imaging of the field distribution in integrated optical waveguides," in *Proc. II IEEE/LEOS Symp. Benelux Chapter*, 1997, pp. 17–20.
[3] D. P. Tsai, H. E. Jackson, R. C. Reddick, S. H. Sharp, and R. J. Warmack, "Photon scanning tunneling microsocope study of optical waveguides," *Appl. Phys. Lett.*, vol. 56, no. 16, pp. 1515–1517, Apr. 1990.
[4] Y. Toda and M. Otshu, "High spatial resolution diagnostics of optical waveguides using a photon-scanning tunneling microscope," *IEEE Photon. Technol. Lett.*, vol. 7, pp. 84–86, Jan. 1995.
[5] S. I. Hosain, J. P. Meunier, E. Bourillot, F. de Fornell, and J. P. Goudonnet, "Review of the basic mehtods for characterizing integrated optic waveguides," *Fiber Integr. Opt.*, vol. 14, pp. 89–107, 1995.
[6] S. Bourzeix, J. M. Moison, F. Mignard, and F. Barthe, "Near-field optical imaging of light propagation in semiconductor waveguides structures," *Appl. Phys. Lett.*, vol. 73, no. 8, pp. 1035–1037, Aug. 1998.
[7] D. H. Naghski, S. M. Lindsay, C. D. Poweleit, G. N. De Bradaber, V. Subramaniam, H. E. Jackson, and J. T. Boyd, "Use of near field optical microscopy (NSOM) to characterize optical channel waveguide structures," in *Proc. SPIE*, vol. 2686, 1996, pp. 64–72.
[8] A. Mannoni, F. Quercioli, B. Tiribilli, C. Ascoli, P. Baschieri, and C. Frediani, "Measuring topography and refractive index of channel waveguides with a hybrid AFM-SNOM," *J. Lightwave Technol.*, vol. 16, pp. 388–394, Mar. 1998.
[9] N. van Hulst, M. Moers, and E. Borgonjen, "Applications of near field optical microscopy," in *Photons and Local Probes*, ser. NATO ASI. New York: Kluwer Academic, 1995, pp. 165–180.
[10] K. Karrai and R. D. Grober, "Piezoelectric tip-sample control for near field optical microscopes," *Appl. Phys. Lett.*, vol. 66, no. 3, pp. 1842–1844, Apr. 1995.
[11] M. A. Paesler and P. J. Moyer, *Near-Field Optics: Theory, Instrumentation, and Applications*. New York: Wiley, 1996, ch. 3, pp. 55–59.
[12] M. A. Duguay, Y. Kokubun, T. L. Koch, and L. Pfeiffer, "Antiresonant reflecting optical waveguides in SiO_2–Si multilayer structures," *Appl. Phys. Lett.*, vol. 49, no. 7, pp. 13–15, July 1986.

X. Borrisé, photograph and biography not available at the time of publication.

D. Jiménez, photograph and biography not available at the time of publication.

N. Barniol, photograph and biography not available at the time of publication.

F. Pérez-Murano, photograph and biography not available at the time of publication.

X. Aymerich, photograph and biography not available at the time of publication.